

**Novel Alpha Cyanocinnamate Derivatives as  
Monocarboxylate Transporter-1 Inhibitors**

**A THESIS**

**PRESENTED TO THE FACULTY OF THE DEPARTMENT OF CHEMISTRY**

**UNIVERSITY OF MINNESOTA, DULUTH**

**BY**

**RYAN J. CONNELL**

**IN PARTIAL FULFILLMENT OF THE REQUIREMENTS FOR THE DEGREE  
OF MASTER OF SCIENCE**

**JULY 2011**

## **ACKNOWLEDGEMENTS**

I wish to express my appreciation and gratitude to Dr. Venkatram R. Mereddy, my thesis advisor, for his valuable advice, constant support and expert guidance. I am also thankful to him for his great amounts of time given to achieve my success in this endeavor. Without his help and guidance throughout my undergraduate and graduate career I would not have achieved all the success that I have had, and I will be forever grateful to him.

I would also like to thank the Department of Chemistry and Biochemistry for its financial support for the past two years. My thanks go to the faculty in the Department of Chemistry and Biochemistry for the knowledge they have taught me during this time. I thank all my group members for their support given me for the past two years.

## ABSTRACT

Ryan J. Connell, Novel  $\alpha$ -Cyanocinnamate Derivatives as Monocarboxylate Transporter-1 Inhibitors, Master of Science (Department of Chemistry and Biochemistry), University of Minnesota.

Tumors contain aerobic and hypoxic regions and hypoxia is associated with an elevated risk of local advancement and metastasis. Hypoxic tumor cells in general, are resistant to chemotherapy and radiation, leading to treatment failure and patient mortality. Cancer cells under hypoxic conditions convert glucose to lactate and aerobic cancer cells consume the lactate for oxidative phosphorylation. This way, the limited glucose available to the tumor is used most efficiently and this existence of a “metabolic symbiosis” between hypoxic and aerobic cancer cells is crucial for their propagation. The key molecular component in this symbiotic relationship is the monocarboxylate transporter-1 (MCT1).

MCT1 is an integral membrane protein that transports lactate into cancer cells. Cellular expression of MCT1 protein has been detected exclusively in nonhypoxic regions of human cancers. When MCT1 is inhibited, this metabolic symbiosis is disrupted and aerobic cancer cells consume large amounts of glucose rather than lactate leading to the death of hypoxic cancer cells due to glucose deprivation. The purpose of this project involves design, synthesis and validation of novel  $\alpha$ -cyanocinnamate derivatives as MCT-1 inhibitors. We utilized Knoevenagel type condensation of aldehydes with cyanocinnamic acid to synthesize several CHC analogs. These analogs have been evaluated using a cell culture based assay of MCT1 transport function and identified potential lead molecules for further optimization and development. The

potential outcome of this project will be a new class of anti-cancer agents with higher affinity and specificity than previously available.

## TABLE OF CONTENTS

I.	LIST OF SCHEMES	v
II.	LIST OF FIGURES	vi
III.	CHAPTER 1: INTRODUCTION	1
IV.	CHAPTER 2: RESULTS AND DISCUSSION	9
V.	CHAPTER 3: WORKS CITED	30
VI.	CHAPTER 4 EXPERIMENTAL	33
VII.	CHAPTER 5: APPENDIX	51

## **LIST OF SCHEMES**

Procedure 1:	13
Procedure 2:	14
Procedure 3:	14

## LIST OF FIGURES

Figure 1:	Schematic representation of the flow of lactate in tumor cells and in tumor cells in which MCT1 has been inhibited	6
Figure 2:	The role of MCT1 in T cell proliferation	8
Figure 3:	$\alpha$ -Cyano-4-Hydroxy Cinnamate	9
Figure 4:	Phenyl Pyruvate	9
Figure 5:	Quercetin	10
Figure 6:	Phloretin	10
Figure 7:	Quinolinethiophene amide derivative-1	10
Figure 8:	Quinolinethiophene amide derivative -2	10
Figure 9:	Quinolinethiophene amide derivative -3	11
Figure 10:	Modification of CHC	13
Figure 11:	Synthetic scheme using cyanoacetic acid, NaOH, NaHCO <sub>3</sub> , Dioxane	13
Figure 12:	Synthetic scheme using cyanoacetic acid, Piperidine	14
Figure 13:	Synthetic scheme for the substituted benzaldehyde derivative using NH <sub>4</sub> OAc/Toluene	14

Figure 14:	Clinically used anticancer bis-chloroethylamines	19
Figure 15:	Lead molecules established by lactate uptake study	24
Figure 16:	IC <sub>50</sub> of compound <b>11</b>	26
Figure 17:	IC <sub>50</sub> of compound <b>13</b>	27
Figure 18:	IC <sub>50</sub> of compound <b>10</b>	27
Figure 19:	IC <sub>50</sub> of compound <b>16</b>	28
Figure 20:	IC <sub>50</sub> of compound <b>17</b>	28

## CHAPTER 1: INTRODUCTION

### 1.1 MONOCARBOXYLATE TRANSPORTERS

Monocarboxylate Transporters (MCTs) are a member of the solute carrier 16 (SLC16) gene family and there are 14 known MCT isoforms.<sup>1</sup> To date no crystal structures of any MCTs has been solved. However, from the sequence, hydrophobicity plots predict that MCTs contain 12 transmembrane domains, along with the C- and N-termini located in the cytosol.<sup>2, 3</sup> Of the fourteen isoforms of MCTs, only MCT1-4 have been shown to transport monocarboxylates. Such monocarboxylates include lactate, pyruvate, butyrate, and some ketone bodies.<sup>1</sup> Some MCTs require ancillary proteins and some of these proteins may aid in cellular localization but the role is not completely known at this time.<sup>4</sup>

### 1.2 MCT1

MCT1(45kDa) was first discovered in Chinese hamster ovary cells when mevalonate transport was altered, resulting from a point mutation.<sup>1</sup> Since the discovery of MCT1, human, rat, and mouse homologues have been cloned and characterized. In humans, MCT1 is ubiquitously expressed among all tissue types.<sup>1</sup> MCT1 like all MCTs is predicted to contain 12 transmembrane regions per the Kyte-Doolittle algorithm.<sup>5</sup> Kinetics of MCT1 have been studied using radiotracer techniques. Studies were carried out using red blood cells where the only MCT present is the MCT1 isoform therefore, any data pertaining to transport of lactate and pyruvate is a result of MCT1 activity. The mechanism of MCT1 was demonstrated to have an ordered and sequential mechanism. This was done by determination of the effect of pH on the kinetics of the net flux of lactic

acid and lactate exchange.<sup>6,7</sup> In the mechanism, transport was shown to involve a proton initially bonding to MCT1 followed by binding of lactate anion, both are then translocated across the membrane. The process is reversible, equilibrium is reached when  $[\text{lactate}]_{\text{in}}/[\text{lactate}]_{\text{out}}=[\text{H}^+]_{\text{out}}/[\text{H}^+]_{\text{in}}$ . The kinetic constraints of this reaction are modeled using the Haldane equation:

$$(V_{\text{max}}/K_{\text{m}})_{\text{influx}}=(V_{\text{max}}/K_{\text{m}})_{\text{efflux}}$$

The rate of reaction for lactic acid flux then is limited by the amount of free carrier that is returned across the membrane.<sup>5</sup> Considering that the protein functions as an exchanger, it is feasible that transport can occur bidirectionally. Experiments however, have shown that the role of MCT1 is primarily to be involved in the uptake of substrates.<sup>8</sup>

MCT1 is known to transport several biologically relevant substrates such as lactate, pyruvate, and butyrate.<sup>1</sup> Beyond these substrates, MCT1 has been shown to be less specific than originally thought as it transports a wide range of monocarboxylates. It has been shown that  $K_{\text{m}}$  decreases as chain length increases from two to four carbons. In monocarboxylates those that are substituted at C-2 or C-3 are good substrates for MCT1, and those with a carbonyl at C-2 are favored over those with a carbonyl at C-3. When transporting lactate it has been shown that MCT1 is stereospecific in that it will only transport the L-isomer of lactate. However, no such stereospecificity is shown for other monocarboxylates.<sup>5</sup> While lactate and pyruvate are both transported by MCT1, it should be noted that MCT1 has a higher affinity for pyruvate than it does for lactate.<sup>1</sup>

### 1.3 MCT1 and Glycolysis

MCT1 is also linked to glycolysis in the body. In glycolysis, one molecule of glucose is converted into two molecules of ATP and two molecules of pyruvate.<sup>9</sup> Some of the resulting pyruvate enters the citric acid cycle where it is converted into acetyl CoA which ultimately enters oxidative phosphorylation netting 34 ATP.<sup>5</sup> The lactate which is produced under normal conditions is regarded as a waste product of glycolysis, and is transported out of the cell via a monocarboxylate transporter protein. At the end of the process, accounting for both glycolysis and oxidative phosphorylation, the cell can produce 36 ATP. This process differs however, in tissues where a heterogeneous cell population is present.<sup>9</sup>

#### 1.4 MCT1 and Cancer Biology

One such system where a heterogeneous cell population is present is a solid tumor. Indeed, tumors are composed of two cell types. One cell type is proximal to the blood vessel and this is the oxygenated region of the tumor. Distal to the blood vessel are cells which compose the hypoxic region of the cell. Considering the fact that oxygen is less available in the hypoxic region of the tumor than in the aerobic region, those hypoxic cells must develop an alternative method for energy production. Indeed, tumor cells have developed a symbiosis wherein hypoxic cells rely on glycolysis exclusively for energy production, and aerobic cells use lactate from the hypoxic cells to fuel their oxidative phosphorylation.<sup>9</sup> Lack of oxygen is the driving force for this pathway to obtain energy. When hypoxic conditions arise, cells uncouple glycolysis from oxidative phosphorylation meaning that glycolysis becomes the sole pathway for the synthesis of ATP. This adaptation is known as a glycolytic switch which occurs through down regulation of the Pasteur effect, and normally it is only temporary in nature.<sup>9</sup> In some tissues however, the

uncoupling of glycolysis from oxidative phosphorylation becomes permanent. This is known as the Warburg effect and it has been observed in cancer cells and is an established phenomenon of advanced stage cancers.<sup>10</sup> Although glycolysis yields only 2 ATP, not only do hypoxic cells thrive but the glycolytic component of the cells has been shown to be critical to the growth and development of malignant tumors.<sup>9</sup>

The process by which intratumoral hypoxia and the resulting metabolic symbiosis is thought to occur the following way. Tumor cells distal to the blood vessel must adapt to survive under conditions with reduced oxygen. To do this they increase the expression of hypoxia inducing factor 1 (HIF-1). HIF-1 makes it possible for a cell to survive on glycolysis even though it yields 2 ATP because HIF-1 induces expression of proteins that will increase the cells ability to uptake glucose. The proteins that are expressed include glucose transporter 1 (GLUT1) which aids in transporting glucose into the cell. Indeed expression of more GLUT1 may aid in overcoming the deficit of ATP in that more glucose will enter the cell which will allow for more glycolysis to occur and as a result more ATP will be produced. HIF-1 also increases the expression of glycolytic enzymes which take part in the glycolysis reactions by converting glucose to pyruvate. A protein called lactate dehydrogenase-A (LDHA) is also expressed which converts pyruvate to lactate. Very few molecules of pyruvate are able to make their way to the mitochondria as the actions of pyruvate dehydrogenase kinase 1 (PDK-1) are blocked, and the mitochondrial mass is decreased. Lactate that was made is then effluxed from the hypoxic cell via MCT4. The lactate is then influxed into the aerobic cell, aerobic cells have low levels of HIF-1 and therefore, their ability to obtain energy from glycolysis is compromised. Since these cells cannot efficiently utilize glycolysis, they must use the

lactate produced from the hypoxic cells. Lactate is then transported into the aerobic cells via MCT1. Lactate is converted into pyruvate by lactate dehydrogenase-B (LDHB). The resulting pyruvate may then enter the Citric Acid Cycle and ultimately undergo oxidative phosphorylation.<sup>9,11</sup>

This pathway is quite significant in that it presents not only the process that tumors undergo to obtain energy, but it is apparent that tumors obtain energy in a fashion that is on the whole different from the processes of normal cells. Given that we have a somewhat unique property of tumor cells we may seek to exploit these processes for clinical benefit. Indeed the metabolism of a tumor is dependent on the shuttling of lactate between cells and the protein that mediates this transfer is MCT1 along with MCT4. Therefore, these two MCTs are lucrative targets for anti-cancer therapy. It is thought that MCT1 inhibition could work either alone or in tandem with radiotherapy.<sup>9</sup>

MCT1 is expressed in a multitude of cancers including human colon, breast, head and neck, and lung. When MCT1 is blocked by using the MCT1 specific inhibitor  $\alpha$ -cyano-4-hydroxycinnamic acid (CHC) the tumor burden is reduced.<sup>9</sup> The hypothesized model of action for the blockage of lactate uptake and resulting tumor death proceeds as follows. When the MCT1 in the aerobic cells is blocked, lactate is no longer able to be transported into the cell. The absence of lactate presents a problem as the aerobic region has now lost the ability to make pyruvate since the cell undergoes no glycolysis of its own. To compensate for this, the aerobic cells must now import glucose whereas before they didn't need to since the hypoxic region would import glucose and create lactate for the aerobic region. The symbiosis between the two regions is now gone and the aerobic region being closer to the blood vessel is better positioned to take up glucose. When

glucose is taken by the aerobic region, the hypoxic region is without its only energy source and undergoes apoptosis as a result of glucose starvation (Figure 1). This method indirectly kills hypoxic cells which are resistant to conventional chemotherapeutic methods and cause tumor relapse, as the inhibition is on MCT1 found on aerobic cells.<sup>9</sup> Having killed the hypoxic cells the more manageable aerobic cells are left which may be treated using more standard chemotherapeutic methods, or radiotherapy.

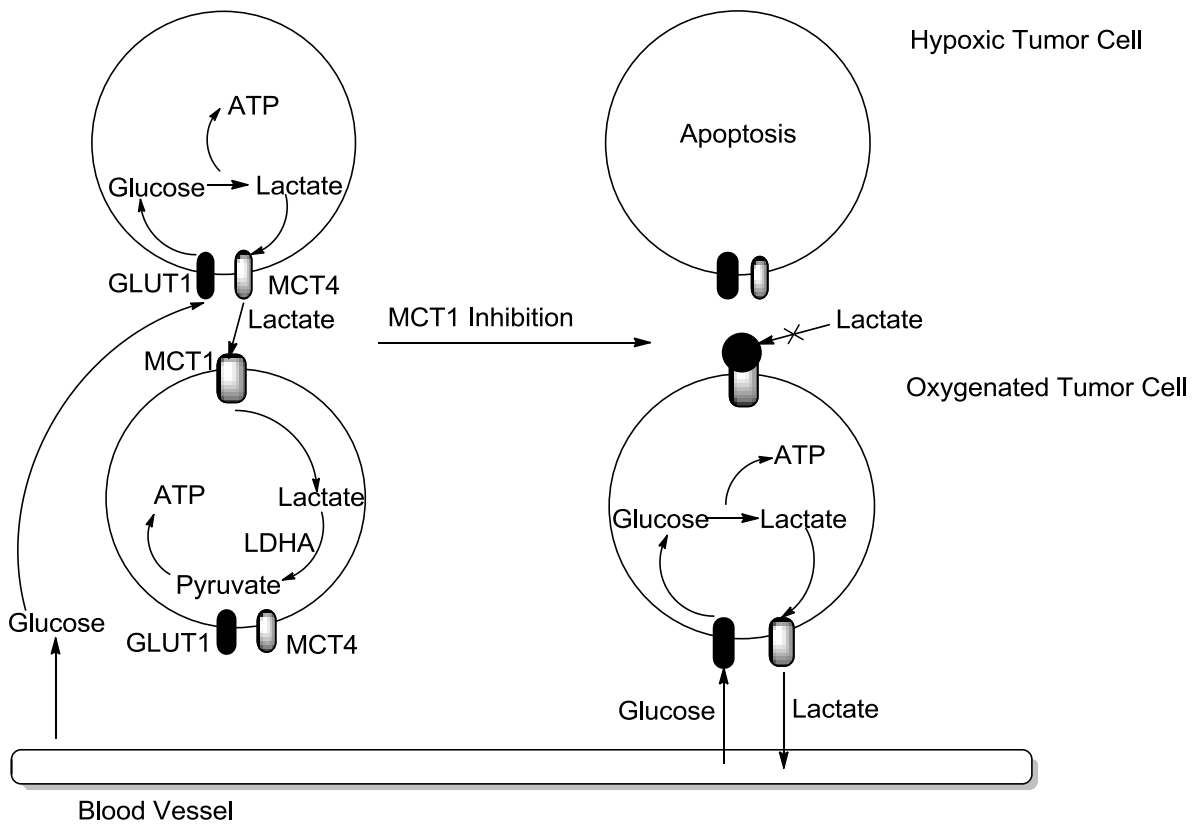


**Figure 1:** Schematic representation of the flow of lactate in tumor cells and in tumor cells in which MCT1 has been inhibited

## 1.5 MCT1 and Immunosuppression

Beyond MCT1 being a lucrative target for anticancer agents, there is also evidence that MCT1 inhibition could be useful as an immunosuppressive strategy. In an immune response, a rapid division of T cells occurs, for the T cells to divide effectively they must become activated. It is known that these activated T cells use glycolysis as their means for energy production. Interestingly they use glycolysis even though the cells exist in an aerobic environment. MCT1 is critical to the cells then as lactate is being produced rapidly and must be exported from the cell accordingly.<sup>12</sup> Indeed, when comparing MCT1 levels in resting T cells as opposed to activated T cells it has been shown that the level of MCT1 expression is greater. Also of note is the different role that MCT1 plays in activated T cells compared to the role it plays in tumor cells. In tumor cells MCT1 is responsible for the influx of lactate as opposed to efflux which is handled by the MCT4 isoform, whereas in activated T cells MCT1 functions to efflux lactate from the cell.<sup>12</sup> T cells use aerobic glycolysis for energy production despite the abundance of oxygen is not completely understood. The reason may be that formation of reactive oxygen species which could damage DNA during a time of heavy DNA synthesis.<sup>13</sup>

As MCT1 plays a critical role in the aerobic glycolysis of the activated T cells by exporting lactate, it is expected that blocking MCT1 will cause a significant rise in the concentration of lactate within the cell. Indeed we see such a relationship, when MCT1 is treated with an inhibitor the lactate levels within the cell rise to three times the level of lactate within an untreated cell ultimately making glycolysis no longer a viable option for energy production.<sup>13</sup> Ultimately it is believed that inhibition of MCT1 leads to a buildup of lactate in the cell and which decreases glycolytic flux effectively limiting the

proliferation of new lymphocytes (Figure 2).<sup>14</sup> Using MCT1 inhibition therapeutically as an immunosuppressing technique does show promise particularly with long term graft survival.

The rate of short term graft survival has been improved by current immunosuppressants but in the past 20 years there has been no improvement in the abilities of the agents to promote long term graft survival.<sup>14</sup> Recently however, agents which inhibit MCT1 have been shown to aid in prolonged allograft survival in rat models. Researchers have in fact, shown that inhibition of MCT1 has prolonged allograft survival, prevents chronic rejection, and induces tolerance in rat allograft models.<sup>14</sup>

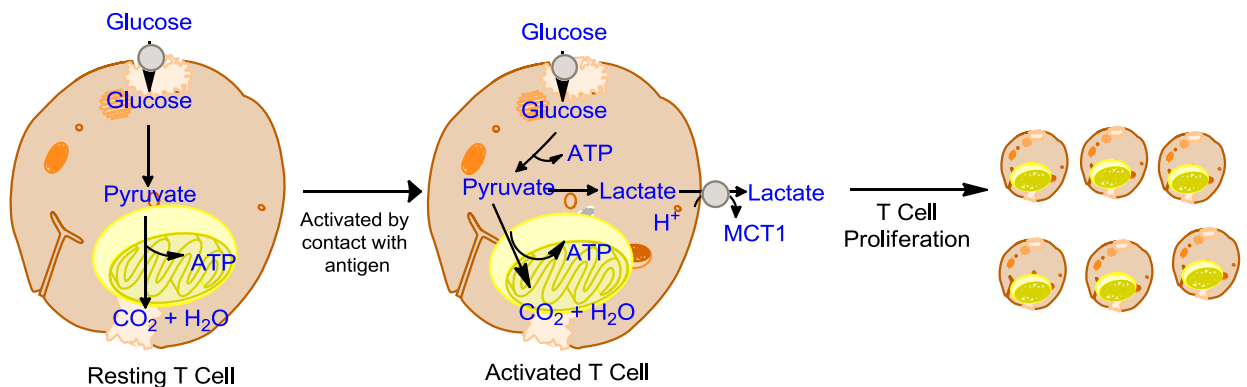


**Figure 2:** The role of MCT1 in T cell proliferation, showing the use of glycolysis and the role of lactate in energy production.

## CHAPTER 2: RESULTS AND DISCUSSION

### 2.1 Inhibitors of MCT1

There are few inhibitors of MCT1 reported in the literature and they can fit into three categories. One category contains compounds which are aromatic monocarboxylates and examples of these include  $\alpha$ -cyano-4-hydroxycinnamate<sup>1</sup> (CHC, Figure-3) and phenylpyruvate<sup>1</sup> (Figure-4). Another category is polyhydroxylated phenolic compounds and examples include quercetin<sup>1</sup> (Figure-5) and phloretin<sup>1</sup> (Figure 6). 4,4'-substituted stilbene-2,2'-disulfonates have also been reported to be MCT inhibitors.<sup>4</sup> Recently AstraZeneca reported quinolinethiophene amide based molecules as potent MCT-1 inhibitors<sup>32,33</sup> (Figures-7-9).

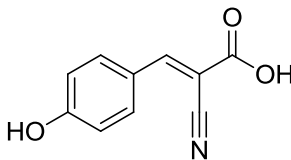


**Figure 3:**  $\alpha$ -cyano-4-hydroxycinnamate

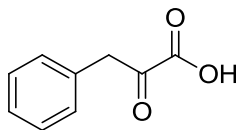


**Figure 4:** Phenyl Pyruvate

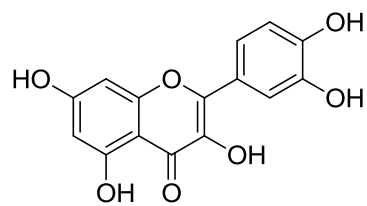


**Figure 5:** Quercetin

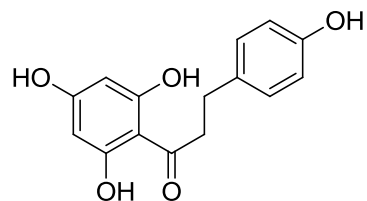


**Figure 6:** Phloretin

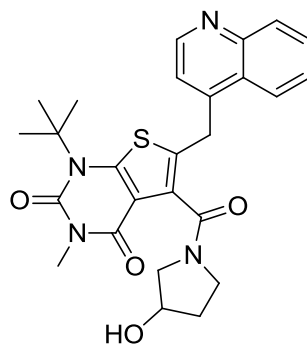


**Figure 7:** Quinolinethiophene amide derivative introduced by AstraZeneca

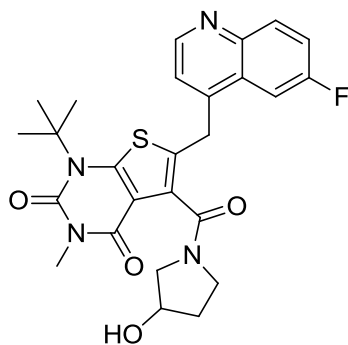


**Figure 8:** Quinolinethiophene amide derivative introduced by AstraZeneca

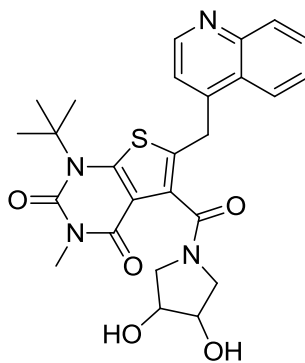


**Figure 9:** Quinolinethiophene amide derivative introduced by AstraZeneca

**Hypothesis:** The lactate produced by hypoxic cancer cells via glucose metabolism is consumed by aerobic tumor cells for use as a substrate for oxidative phosphorylation. Thus, the limited glucose available to the tumor is used most efficiently via a synergistic metabolic symbiosis. Hypoxic cells also down regulate oxidative phosphorylation in order to maintain redox homeostasis and accordingly, take up large amounts of glucose to maintain energy homeostasis. The expression of MCT1 in aerobic cancer cells leads to the efficient uptake of lactate followed by lactate dehydrogenase B (LDHB) mediated oxidative conversion to pyruvate. This prevents the aerobic cells from consuming large quantities of glucose via the utilization of lactate as an energy substitute for survival. Inhibition of MCT1 causes the aerobic cancer cells to take up glucose instead of lactate, thereby resulting in the death of hypoxic cancer cells due to glucose deprivation (Figure 1). MCT1 is over expressed in a variety of cancers including brain, breast, head, neck, lung, colon, etc. Since tumor cells induce these transporters specifically for their unique metabolic needs, we hypothesize that normal cells would be relatively immune to the chemotherapeutic actions thereby leading to minimal side effects. Thus, MCT1 inhibition in combination with standard chemo/radiotherapy has tremendous potential as a novel complimentary and synergistic protocol for treating cancers.

$\alpha$ -Cyano-*p*-hydroxycinnamate (CHC) is reported as selective MCT1 inhibitors with  $K_i$  value in  $>100\mu\text{M}$  range, and is not significantly cytotoxic. Considering the selective MCT1 inhibitory profiles of CHC (*albeit* at higher concentrations) coupled with its simple chemical structure, we envision to synthesize and evaluate several CHC analogs to understand the structure activity relationship and obtain lead molecules that inhibit MCT1 at low nanomolar concentrations for potential development as targeted *anti*-cancer agents.

**Specific Aims:** The purpose of this project was to validate the hypothesis that MCT-1 inhibitors could be utilized as targeted and complementary *anti*-cancer agents. The specific aims of this project are (1) to design and synthesize novel small molecules as MCT-1 inhibitors, (2) *in vitro* and *in vivo* biological evaluation of the potent MCT-1 inhibitors as single agent anticancer agents or complementary synergistic agents in combination with primary chemotherapeutic agents.

### **Design and Synthesis of $\alpha$ -Cyano-4-hydroxycinnamate (CHC) Derivatives as MCT1 Inhibitors**

CHC can be modified at several places at CN, COOH, olefin, phenyl ring and hydroxyl group. We chose the phenyl ring modification for the current study. We systematically investigated the ring activation and ring deactivation by introducing the electron donating and electron withdrawing groups.

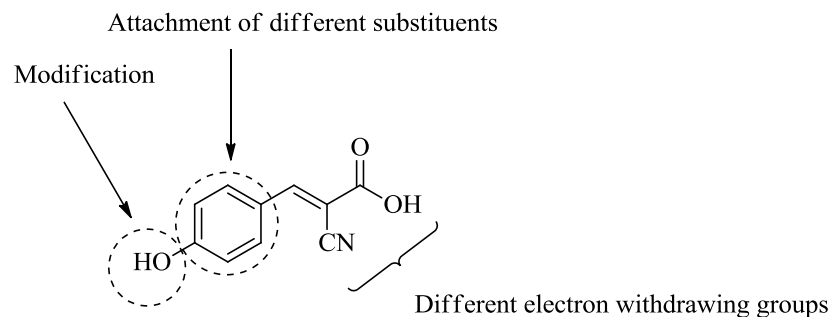


**Figure 10:** Modification of CHC

Our synthesis involved three variations of the Knoevenagel condensation. We first attempted synthesis using procedure 1 (Figure 11), if no reaction occurred or poor yields were observed we moved onto procedure 2 (Figure 12), and finally if procedure 2 was unsuccessful we moved on to procedure 3 (Figure 13).

**Procedure I:**

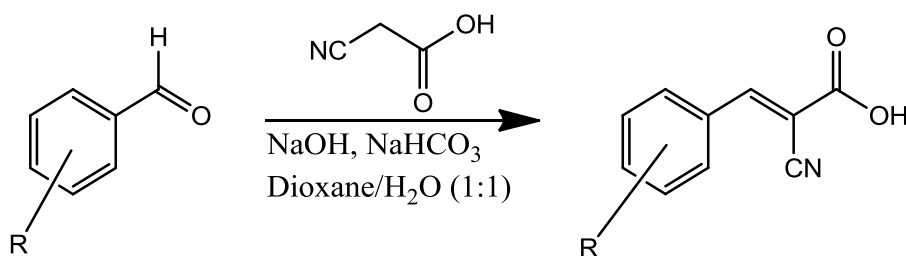


**Figure 11:** Synthetic scheme using cyanoacetic acid, NaOH, NaHCO<sub>3</sub>, Dioxane, water

R= -OMe, -(OMe)<sub>3</sub>, -Piperanal derivative, -Vanilin benzaldehyde derivative, -F, -Br (para), -Br (meta), -Br (ortho), -N<sub>2</sub>O, -CN, -CH<sub>2</sub>OH

### Procedure II:

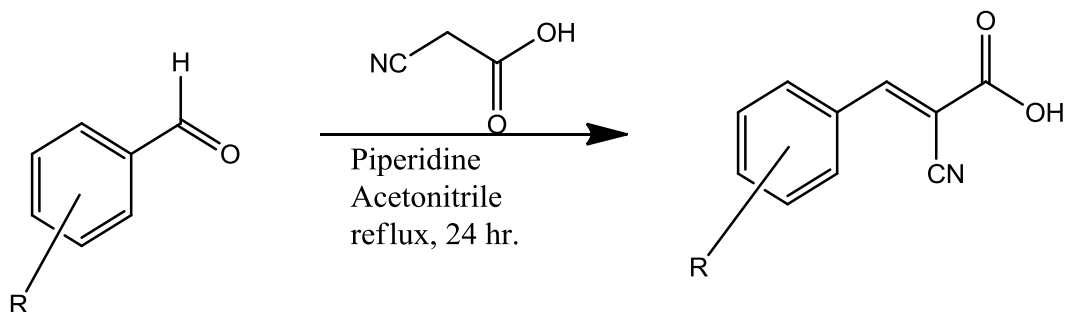


**Figure 12:** Synthetic scheme using cyanoacetic acid, piperidine

R= C<sub>6</sub>H<sub>4</sub>, -N(CH<sub>3</sub>)<sub>2</sub>, -N(C<sub>2</sub>H<sub>5</sub>)<sub>2</sub>, -N(C<sub>2</sub>H<sub>4</sub>Cl)<sub>2</sub>, 4-pyridine, 3-pyridine

### Procedure III:

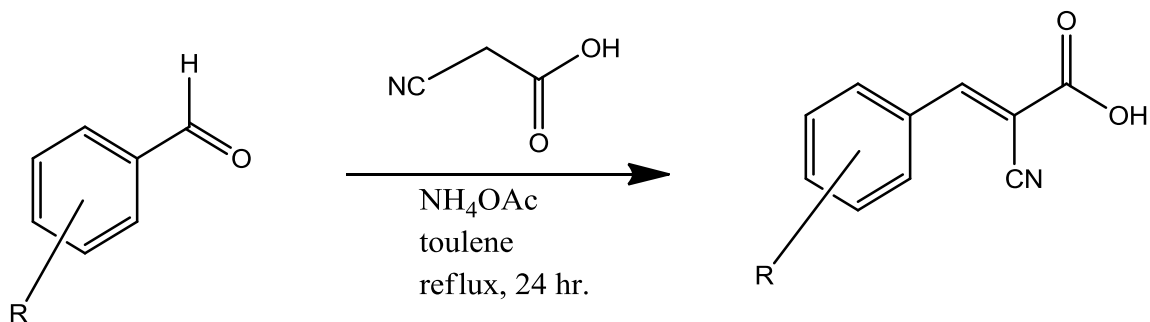


**Figure 13:** Synthetic scheme for the substituted benzaldehyde derivative using NH<sub>4</sub>OAc/toluene

R= -CH<sub>3</sub>, -C<sub>2</sub>H<sub>5</sub>, -CH(CH<sub>3</sub>)<sub>2</sub>

We first started with electron donating groups and in this regard, our initial examples included commercially available p-methoxy benzaldehyde, 3, 4, 5-trimethoxy benzaldehyde and piperonal benzaldehyde. The Knoevenagel condensation of these aldehydes with cyanoacetic acid in the presence of NaOH, NaHCO<sub>3</sub>, dioxane and water provided the corresponding  $\alpha$ -cyanocinnamic acids **1-3** in excellent chemical yields.

Recrystallization of these compounds in 10%EtOAc/Hexane provided the analytically pure compounds and they have been characterized by  $^1\text{H}$ ,  $^{13}\text{C}$  and elemental analysis. Similarly, MeO and OH containing aldehyde vanillin provided the cyanocinnamate **4** in excellent yield. Structures and yields of the products are represented below in Table 1.

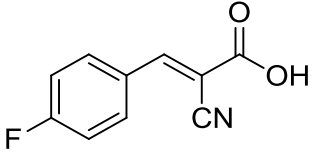
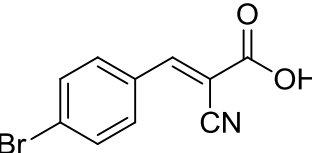
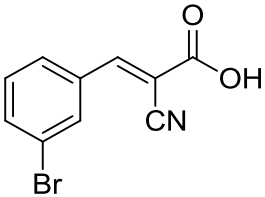
**Table 1:** Methoxybenzaldehyde CHC derivatives

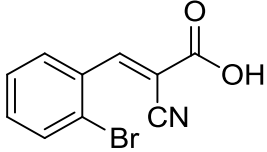
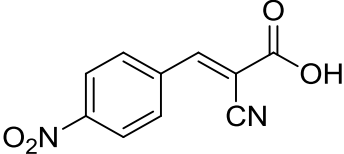
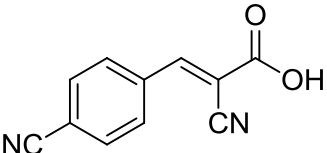
Structure of the Compound	Compound Number	Yield
	<b>1</b>	<b>85%</b>
	<b>2</b>	<b>90%</b>
	<b>3</b>	<b>88%</b>
	<b>4</b>	<b>85%</b>

The examples in the electron withdrawing group include several halogenated aldehydes, nitro and cyano group substituted aldehydes. We began our synthesis in this category by creating derivatives which substituted a halogen for the hydroxyl group on CHC. The first compound we synthesized placed a fluoro group at the para position **5**.

Fluoro groups are generally considered biologically equivalent to hydroxyl groups, and fluoro groups usually increase the pharmacokinetics and pharmacodynamics properties in a compound. We then synthesized a derivative which featured bromo group at the para position **6** so as to increase hydrophobicity, and place a more electron withdrawing group on the molecule. We then made a series of bromo substituted compounds which featured bromine substitutions at the ortho **7**, and meta **8**, positions. Next in our electron withdrawing series, we substituted a nitro and a cyano group at the para position **9** and **10** (Table-2). The synthesis part involved the condensation of the corresponding aldehydes with cyanocinnamic acid in the presence of NaOH, NaHCO<sub>3</sub>. All these compounds were characterized by <sup>1</sup>H, <sup>13</sup>C and elemental analysis.

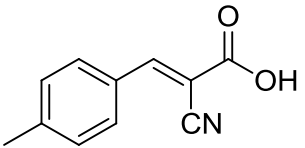
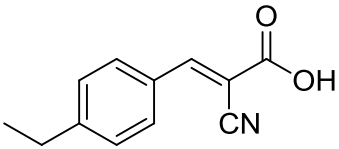
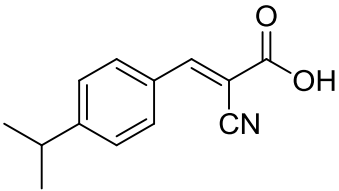
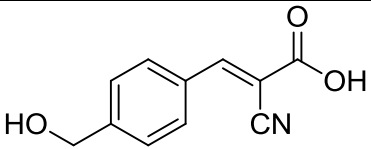
**Table 2:** Electron withdrawing group derivatives (continued on next page)

Structure of the compound	Compound Number	Yield
	<b>5</b>	<b>88%</b>
	<b>6</b>	<b>86%</b>
	<b>7</b>	<b>85%</b>

	<b>8</b>	<b>87%</b>
	<b>9</b>	<b>89%</b>
	<b>10</b>	<b>87%</b>

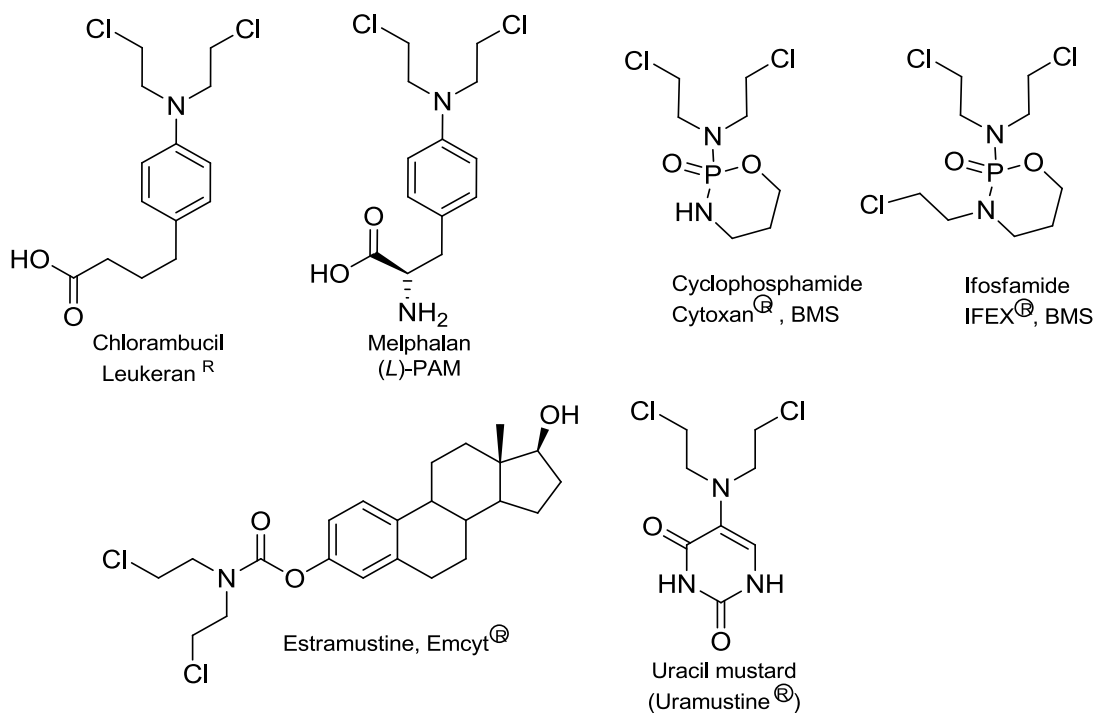
We then moved on to make derivatives with alkyl groups to see what the increased hydrophobicity would do in terms of biological activity. In this category, we chose three aldehydes p-methylbenzaldehyde (tolualdehyde), p-ethylbenzaldehyde, and p-isopropylbenzaldehyde as preliminary examples. Condensation of these aldehydes with cyanocinnamic acid in the presence of  $\text{NH}_4\text{OAc}$  provided the maximum yields of cyanocinnamates **11-13**. We also included 1-naphthaldehyde as an example with an extra aromatic ring and synthesized the corresponding cyanocinnamate **14** in 90% yield (Table-3). Lastly in the series, we extended the hydroxyl group by one carbon **15** from the ring just to see if that had any bearing on the biological activity. This particular hydroxymethyl aldehyde was obtained by partial reduction of terephthalaldehyde with  $\text{NaBH}_4$ .

**Table 3:** Alkyl/Aryl CHC derivatives

Compound Structure	Compound Name	Yield
	<b>11</b>	<b>90%</b>
	<b>12</b>	<b>90%</b>
	<b>13</b>	<b>85%</b>
	<b>14</b>	<b>90%</b>
	<b>15</b>	<b>85%</b>

Nitrogen atom plays a key role in biological activity of many drugs and almost 75% of the clinically used drugs have at least one nitrogen atom in it. We replaced the p-OH group in CHC with dimethylamino and diethylamino groups. The cyanocinnamates **16**, **17** were synthesized from the aldehydes N,N-dimethyl benzaldehyde, and N,N-diethylbenzaldehyde using cyanocinnamic acid and piperidine. We also included bis-chloroethyl amine-CHC derivative **18**. Bis-chloroethyl amines (nitrogen mustards) are

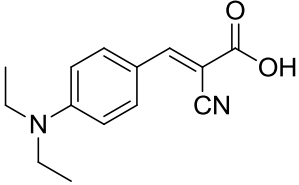
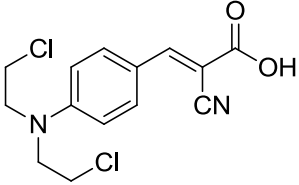
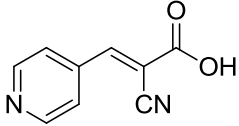
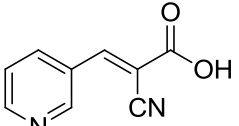
powerful DNA alkylators and many of these derivatives are clinically utilized as anti-cancer agents (Figure 14). Finally, we synthesized two nitrogen containing cyanocinnamates **19** & **20** derived from 2- and 3-pyridine aldehydes (Table-4).



**Figure 14:** Clinically used anticancer bis-chloroethylamines

**Table 4:** N, N-Dialkylamine / Pyridine CHC derivatives (continued on next page)

Structure of the compound	Compound Number	Yield
	<b>16</b>	<b>88%</b>

	<b>17</b>	<b>87%</b>
	<b>18</b>	<b>87%</b>
	<b>19</b>	<b>85%</b>
	<b>20</b>	<b>84%</b>

### **BIOLOGICAL RESULTS:**

After synthesizing the above mentioned CHC derivatives, we evaluated their biological evaluation by performing studies to test their ability to inhibit cellular lactate uptake (Figure 15). From these studies we were able to get interesting insights into the effectiveness of our inhibitors. MCT1 transport inhibition was assessed by measuring the inhibition of lactate uptake by a rat brain endothelial cell line (RBE4) that expresses only MCT1 by a method similar to that described previously.<sup>34</sup> Briefly, confluent cultures of RBE4 cells in 24 well plates were washed 2 times with minimal buffer (HEPES) and then incubated with test compound in minimal buffer containing 3 $\mu$ M [<sup>14</sup>C]-lactate and 5 $\mu$ M lactate. After 15 min, influx was stopped by washing 3 times with ice-cold buffer containing 0.1 mM  $\alpha$ -cyano-4-hydroxycinnamate (CHC), a MCT1 inhibitor. The cells

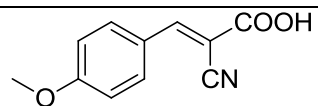
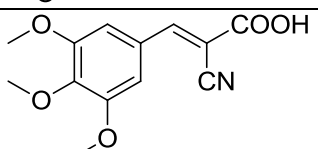
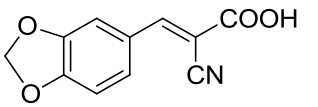
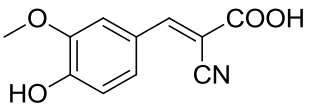
were lysed in 0.1 M NaOH containing 5% Triton X-100 and an aliquot taken from each well for measuring radioactivity using liquid scintillation. Control wells were used for protein analysis by the Bradford assay. Transport was normalized to protein content and expressed as nano mole lactate/mg protein/15 min. Each assay was run in triplicate and the mean value calculated and compared to the inhibition by 0.1 $\mu$ M CHC as a control. Significance for differences between control and test samples was determined using 1-way ANOVA. For the compounds exhibiting inhibition greater than CHC, further assays were conducted at more dilute concentrations such as 0.02 mM and below. These compounds will be considered lead compounds and serve as templates for further chemical synthesis modification for evaluation as potent and specific MCT1 inhibitors.

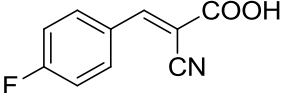
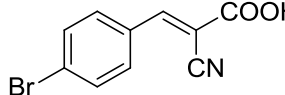
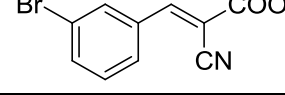
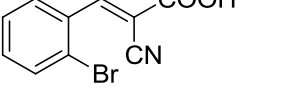
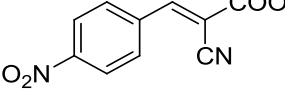
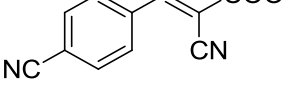
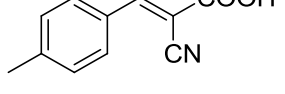
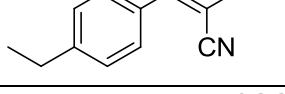
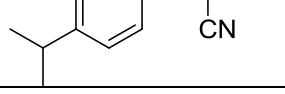
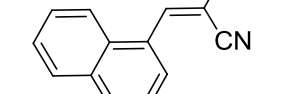
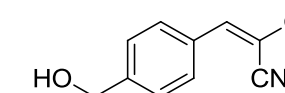
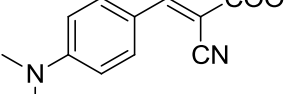
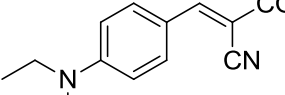
We first tested the cyanocinnamates containing electron donating groups (**1-4**) and the methoxy cinnamate **1** was found to be more potent than the parent CHC. The IC<sub>50</sub> of **1** was 2 $\mu$ M as opposed to 150  $\mu$ M exhibited by CHC. The trimethoxy derivative **2** and pipernal derivative **3** also exhibited more potency than CHC with IC<sub>50</sub> values at 5 $\mu$ M. Surprisingly the vanillin derivative **4** didn't show good activity with IC<sub>50</sub> value at 100 $\mu$ M. All the electron withdrawing group containing cyanocinnamates that we tested showed more potency than CHC with activities ranging from 4  $\mu$ M to 7  $\mu$ M (Table 6). The alkyl derivatives also showed good activity with the isopropyl derivative **13** having an IC<sub>50</sub> value at 281 nM, the toluene derivative was less active with an IC<sub>50</sub> at 812 nM. The ethyl derivative **12** exhibited the intermediary activity at 540 nM. Based on these initial studies, the alkane derivatives have shown promise and warrants synthesis of more derivatives with greater chain length to understand the structure activity studies. The *N,N*-dialkyl amino derivatives showed the best activities with the *N,N*- diethyl amino

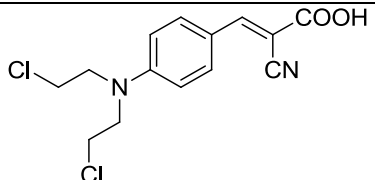
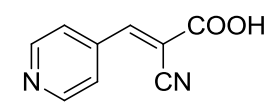
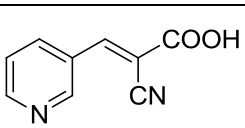
derivative **17** showing the greatest activity with an  $IC_{50}$  of 66 nM. The next most active was also an *N,N*-dimethyl derivative **16** which showed an  $IC_{50}$  of 251 nM. In the future it would be interesting to synthesize more *N,N*-dialkyl amino compounds while increasing the chain length to see if the trend of more activity continues. The bischloroethylamine derivative **18** showed potent activity with an  $IC_{50}$  at 500nM. We also tested lactate uptake activity of clinical anticancer drug chlorambucil and this did not show any MCT-1 inhibitory activity even at 100  $\mu$ M. This study confirms the role of cyanocinnamate moiety in providing the MCT-1 inhibitory activity. It will be interesting to see, if this derivative **18** could be used as targeted anticancer agent for MCT-1 expressing cancers considering the success of other compounds with the nitrogen mustard moiety.

Interestingly, neither of the pyridine derivatives (**19** & **20**) showed any activity at a concentration of 100 $\mu$ M. They had uptake values of 100.9% and 109.6% respectively.

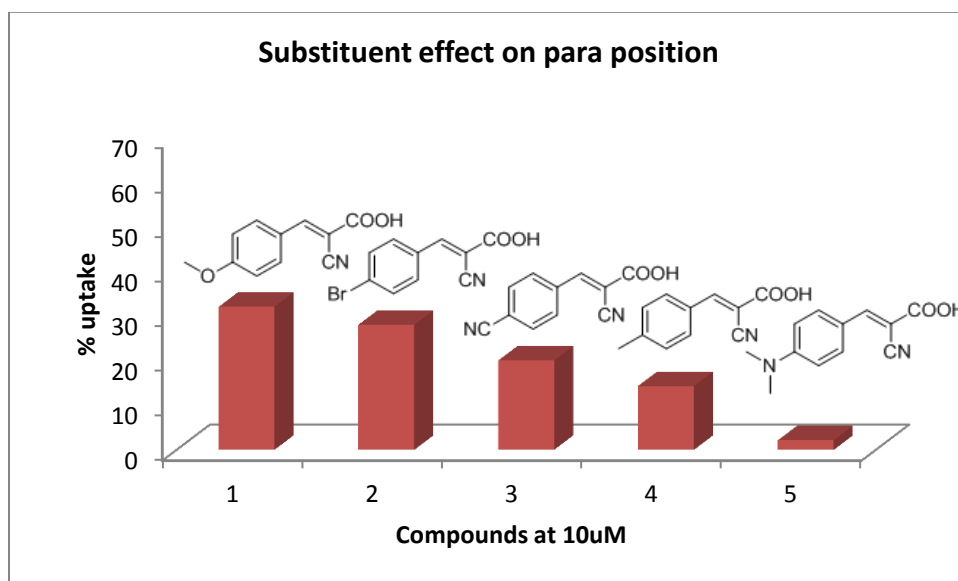
**Table 5:** Lactate uptake values for the synthesized compounds (continued on next page)

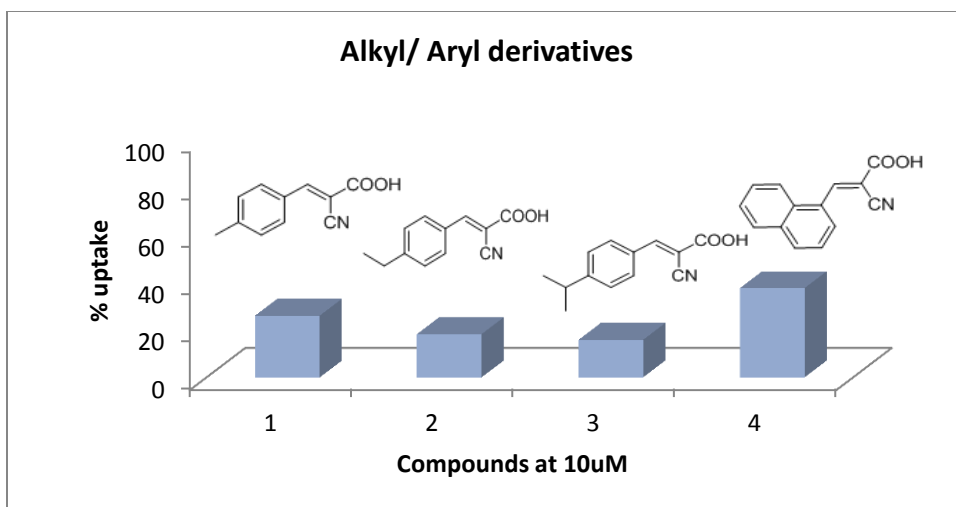
Sl.No	Compound	Concentration	% Uptake
1		10 $\mu$ M	32
2		10 $\mu$ M	75.6
3		10 $\mu$ M	20
4		100 $\mu$ M	51

5		10 $\mu$ M	42.1
6		10 $\mu$ M	28
7		10 $\mu$ M	37
8		100 $\mu$ M	2.67
9		ND	ND
10		10 $\mu$ M	15
11		10 $\mu$ M	14.3
12		10 $\mu$ M	17.2
13		10 $\mu$ M	6.8
14		10 $\mu$ M	23.2
15		100 $\mu$ M	100
16		1 $\mu$ M	23.42
17		1 $\mu$ M	4.4

18		10 $\mu$ M	9.4
19		100 $\mu$ M	>100
20		100 $\mu$ M	>100

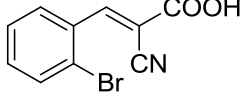
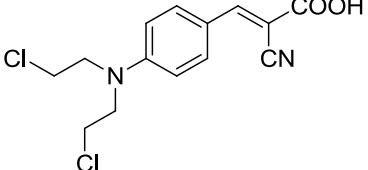
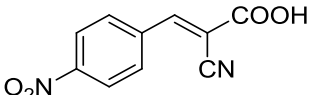
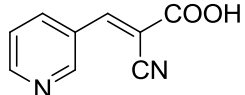
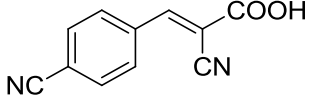
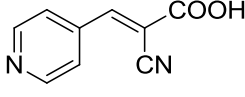
**Figure 15:** Trends in activity with different functional groups





**Table 6:** IC<sub>50</sub> values (ND=not determined)

Sl.no	Compounds	IC-50	Sl.no	Compounds	IC-50
1		2 μM	11		812 nM
2		3 μM	12		540 nM
3		3 μM	13		281 nM
4		100 μM	14		ND
5		ND	15		NA
6		5 μM	16		251 nM +/- 20
7		5 μM	17		66 nM +/- 2

8		ND	18		500nM +/- 0.1
9		ND	19		NA
10		4μM	20		NA

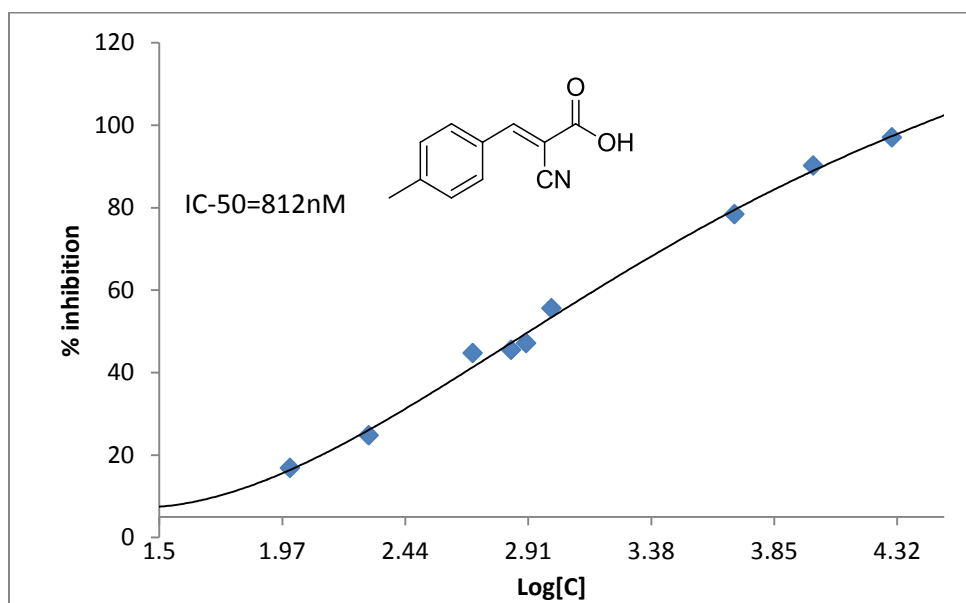


**Figure 16:** IC<sub>50</sub> of compound 11

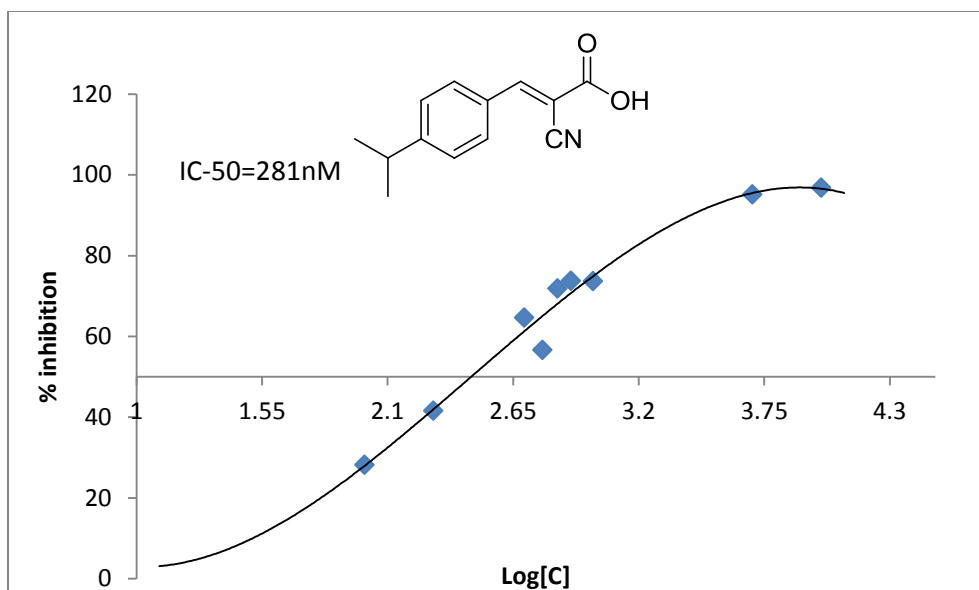


**Figure 17:** IC<sub>50</sub> of compound 13

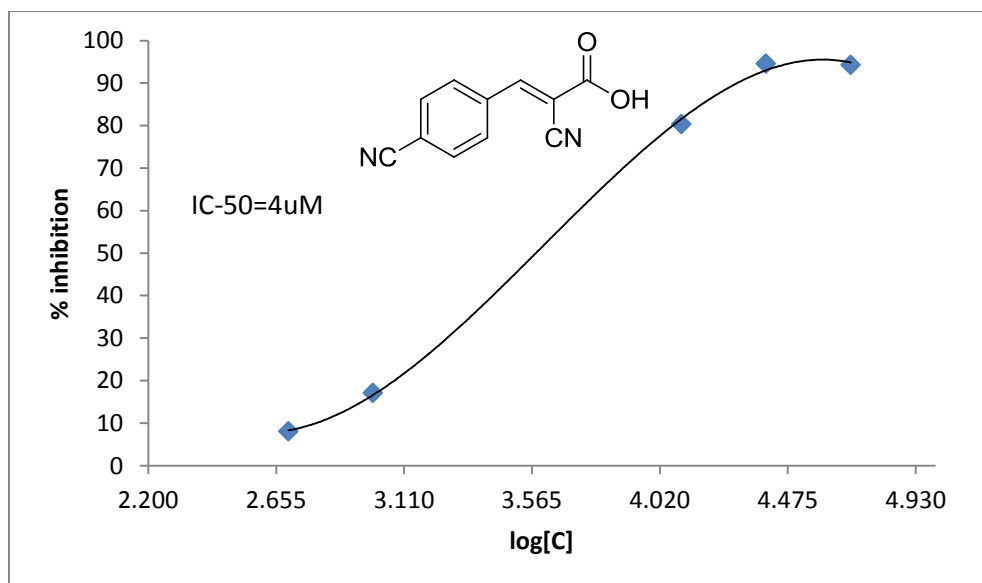


**Figure 18:** IC<sub>50</sub> of compound 10

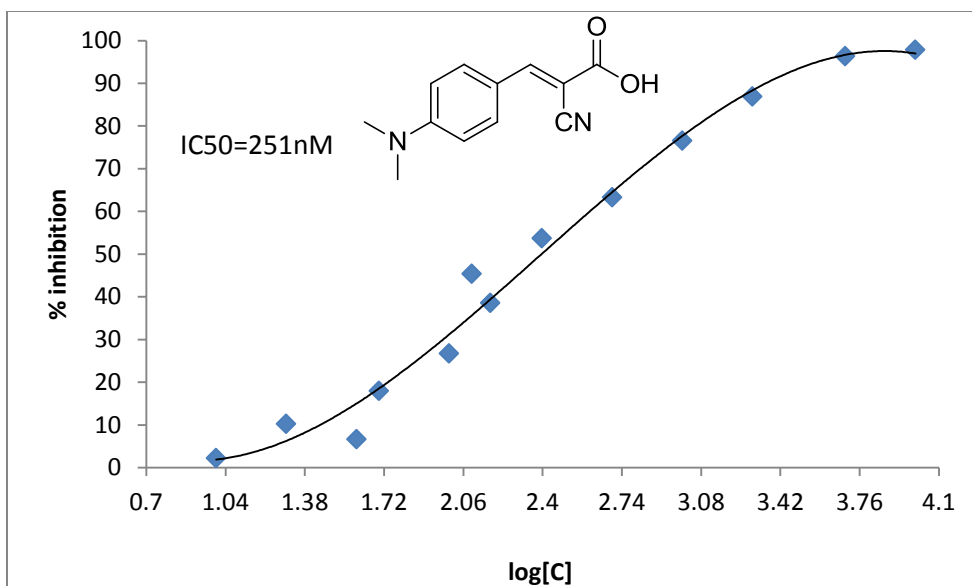


**Figure 19:** IC<sub>50</sub> of compound 16

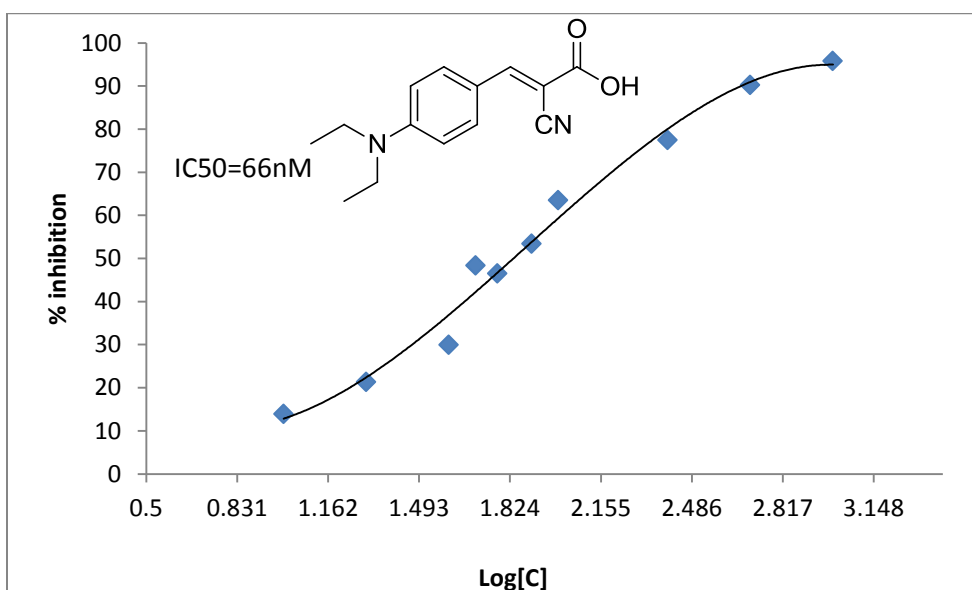


**Figure 20:** IC<sub>50</sub> of compound 17

**Conclusion:**

In conclusion, we synthesized several CHC derived cyanocinnamates via Knoevenagel condensation of aldehydes with cyanocinnamic acid in the presence of a base. All the synthesized molecules were evaluated for their MCT-1 inhibition properties utilizing RBE4 cell lines. In general, several molecules containing electron donating and electron withdrawing groups showed increased potency than parent CHC. *p-N,N*-dialkyl substituted molecules showed the highest activity. We have synthesized one derivative containing the nitrogen mustard. Future studies would include optimization of the lead molecules to further understand the structure activity relationship. We also plan to evaluate the potent molecules for therapeutic applications such as anticancer therapy.

### CHAPTER 3: WORKS CITED

1. Drewes, L.R.; Spanier, J.A.; *Drug Transporters*, **2007**, 147-170.
2. Halestrap, A.P.; Price, N.T. *Biochem J.* **1999**, *343*, 281-289.
3. Halestrap, A.P.; Meredith D.; *Dfluser Arch.* **2004**, *44*, 619-628.
4. Morris, M. E.; Felmlee M. A.; *AAPS Journal* **2008**, *10*, 311-321.
5. DeBrunjin A.W.; Vreeberg H.; Vanseverick J; *Bichim. Biophys Acta* **1983**, *732* 562-568.
6. DeBrunjin A.W.; Vreeberg H.; and Vanseverick J.; *Bichim. Biophys Acta* **1985**, *812*, 841-844.
7. Juel, C.; Halestrap A. P.; *J. Physiol.* **1999**, *517*, 633-642.
8. Sonveaux, P.; Vegran, F.; Schroeder, T.; Wergin, M.; Verrax, J.; Rabbani, Z.; De Saedeleer, C.; Kennedy, K.; Diepart, C.; Jordan, B.; Kelley, M.; Gallez, B.; Wahl, M.; Feron, O.; Dwhirst, M.; *Journal of Clinical Investigation* **2008**, *118*, 3930-3942.
9. Warburg, O.; *Constable*, **1930**, 327
10. Semenza G.; *Journal of Clinical Investigation.* **2008**, *118*, 20-27.
11. Donald, D. K.; Murry, C. M.; Hutchenson, R.; Bantik, J. R.; Belfield, G. P.; Benjamin, A. D.; Cook, D. ;Edwards, S; Holness, E.; Wright, A.; Wilkinson, D. J.; *Nature Chemical Biology* **2005**, *1*, 371-376.
12. Broer, S.; *Nature Chemical Biology*, **2005**, *1*, 356-357.
13. Cho, K.; Yamada, T.; Wynn, C.; Behanna, H. A.; Hong, I. C.; Manaves, V.; Nakanishi T.; Hirose J.; Abi, H.; Tamura, K.; Saita Y.; *Transplantation* **2010**, *90*, 1299-1306.

14. Toshihide, K.; Mamoru, S.; Takeshi, W.; *Tetrahedron Letters* **2007**, *48*, 1972-1976.
15. Poole, R. C.; Bowden N. J.; Halestrap, A. P.; *Biochemical Pharmacology* **1993**, *45*, 1621-30.
16. Poole, R. C.; Cranmer, S. L.; Halestrap, A. P.; Levi, A. J. *Biochemical Journal* **1990**, *269*, 827-9.
17. Hahn, E. L.; Halestrap, A. P.; Gamelli, R. L.; *Shock* **2000**, *13*, 253-60.
18. Schneider, U.; Poole, R. C.; Halestrap, A. P.; Grafe, P.; *Neuroscience* **1993**, *53*, 1153-62.
19. Poole, R. C.; Halestrap, A. P.; Price, S. J.; Levi, A. J.; *The Biochemical Journal* **1989**, *264*, 409-18.
20. Edlund, G. L.; Halestrap, A. P.; *The Biochemical Journal* **1988**, *249*, 117-26.
21. Halestrap, A. P.; Armston, A. E.; *The Biochemical Journal* **1984**, *223*, 677-85.
22. Jackson, V. N.; Halestrap, A. P.; *Journal of Biological Chemistry* **1996**, *271*, 861- 8.
23. Poole, R. C.; Bowden, N. J.; Halestrap, A. P.; *Biochemical Pharmacology* **1993**, *45*, 1621-30.
24. Wang, X.; Poole, R. C.; Halestrap, A. P.; Levi, A. J.; *Biochemical Journal* **1993**, *290*, 249-58.
25. Poole, R. C.; Cranmer, S. L.; Halestrap, A. P.; Levi, A. J.; *Biochemical Journal* **1990**, *269*, 827-9.
26. Poole, R. C.; Halestrap, A. P.; Price, S. J.; Levi, A. J.; *Biochemical Journal* **1989**, *264*, 409-18.

27. Thorsten, J. W.; Karas, M.; Roth, U.; Steinert, K.; Menzel, C.; Reihls, K.; *Journal of the American Chemical Society Mass Spectrum* **2009**, *20*, 1104.
28. Guile, S. D.; Bantick, J. R.; Cooper, M. E.; Donald D. K.; Eyssade, C.; Ingall, A.; Lewis Richard J. M.; Barrie, P. M.; Rukhsana, T. P.; Reynolds, T.J.; Tachel, H.; Andrew D.; *J. Med. Chem.* **2007**, *50*, 254-263.
29. Donald, D. K.; Murry, C. M.; Hutchenson, R.; Bantik, J. R.; Belfield, G. P.; Benjamin, A. D.; Cook, D.; Edwards S.; Holness E.; Wright, A.; Wilkinson, D. J.; *Nature Chemical Biology* **2005**, *1*, 371-376.
30. Ovens, M. J.; Halestrap, A. P.; *Biochem. J.* **2010**, *431*, 217–225.
31. Gottlieb, E.; *Nature Reviews Cancer* **2010**, *10*, 267-277.
32. Smith, J.P.; Drewes, L.R.; *J. Biol. Chem.* **2006**, *281*, 2053-2060.
33. Shimizu, M.; *J. Agric. Food Chem.* **2003**, *51*, 7296-7302
34. Saroj P.; Mathupala.; *Neurosurgery* **2004**, *55*: 1410-1419.
35. Dian W.; Gallagher, S. M.; Castorino J. J.; *Cancer Res.* **2007**, *67*, 4182-4189.
36. Smith, J.P.; Drewes, L.R.; *J. Biol. Chem.* **2006**, *281*, 2053-2060.

## CHAPTER 4: EXPERIMENTAL

### Procedure I:

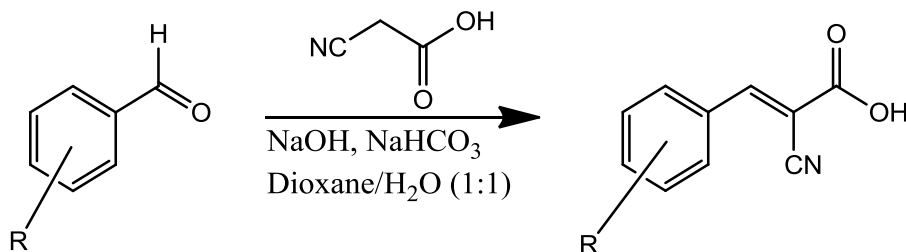


**Figure 11:** Synthetic scheme using cyanoacetic acid, NaOH, NaHCO<sub>3</sub>, Dioxane, water

R= -OMe, -(OMe)<sub>3</sub>, -Piperanal derivative, -Vanilin benzaldehyde derivative, -F, -Br (para), -Br (meta), -Br (ortho), -N<sub>2</sub>O, -CN, -CH<sub>2</sub>OH

10 mmol of the starting substituted benzaldehyde derivative was dissolved in 20 ml of dioxane. 15 mmol of cyanoacetic acid was dissolved in 10 ml of water and 10 ml of dioxane. 15 mmol of both NaOH, and NaHCO<sub>3</sub> were added. The reactants were stirred at room temperature for a period of 24 hours. The product was then precipitated using 3M HCl, filtered and washed with water. Purification was carried out via recrystallization using 10% EtOAc/Hexane.

**Procedure II:**

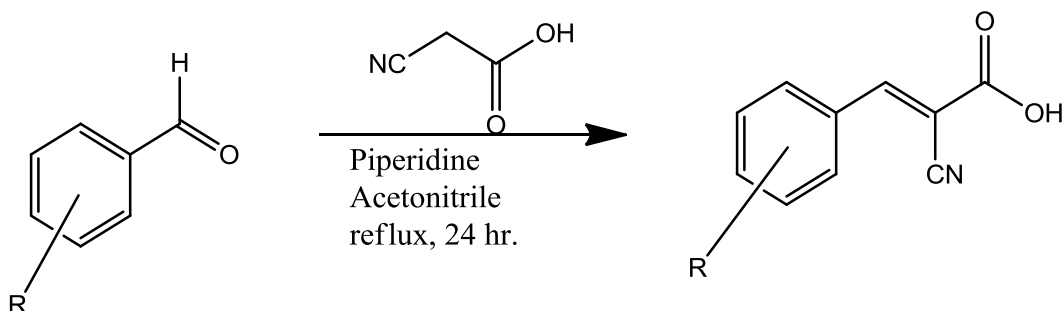


**Figure 12:** Synthetic scheme using cyanoacetic acid, piperidine

R= C<sub>6</sub>H<sub>4</sub>, -N(CH<sub>3</sub>)<sub>2</sub>, -N(C<sub>2</sub>H<sub>5</sub>)<sub>2</sub>, -N(C<sub>2</sub>H<sub>4</sub>Cl)<sub>2</sub>, 4-pyridine, 3-pyridine

10 mmol of the starting substituted benzaldehyde derivative was dissolved in 20 ml of acetonitrile. 15 mmol of cyanoacetic acid was added along with 0.5 ml of piperidine. The reaction mixture was then set to reflux for 24 hrs. The product was then precipitated by adding 25 ml of 3M HCl, filtered and washed with water. Purification was carried out via recrystallization using 10% EtOAc/Hexane.<sup>28</sup>

**Procedure III:**

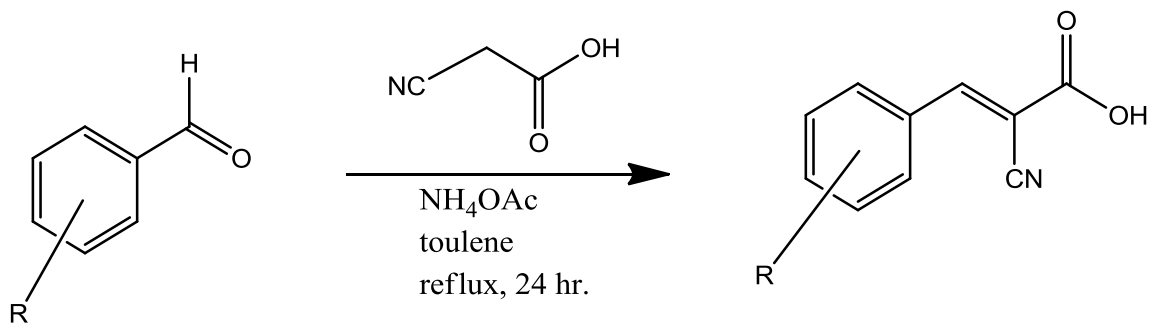


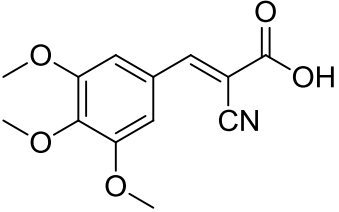
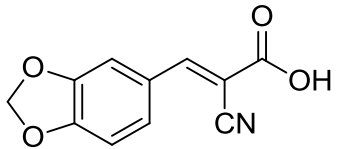
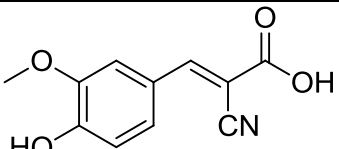
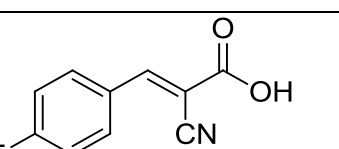
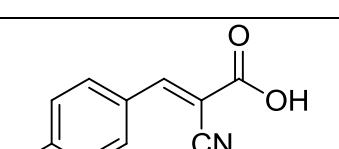
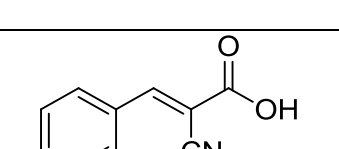
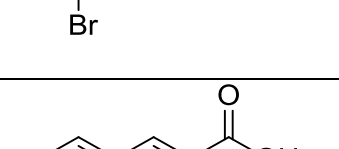
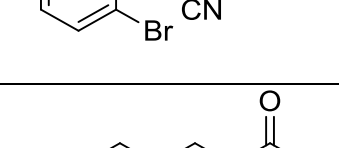
**Figure 13:** Synthetic scheme for the substituted benzaldehyde derivative using NH<sub>4</sub>OAc/toluene

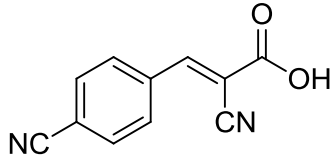
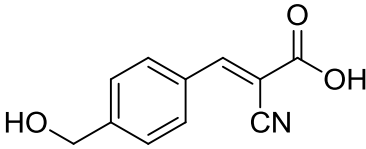
R = -CH<sub>3</sub>, -C<sub>2</sub>H<sub>5</sub>, -CH(CH<sub>3</sub>)<sub>2</sub>

10 mmol of the substituted benzaldehyde derivative was dissolved in toluene, 15 mmol of cyanoacetic acid and 2 mmol of NH<sub>4</sub>OAc was then added and the reaction was allowed to reflux for 24 hrs. The reaction mixture was filtered and washed with water followed by recrystallization from 10% MeOH/water.<sup>29</sup>

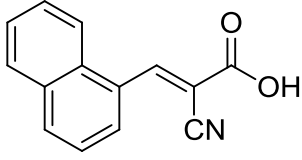
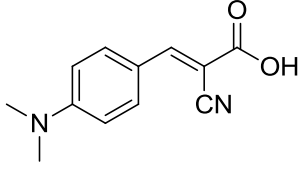
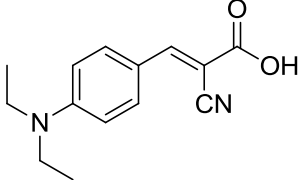
**Table 7:** Products yielded from procedure 1 along with amount of starting material used, and amount of final product formed (continued on next page)

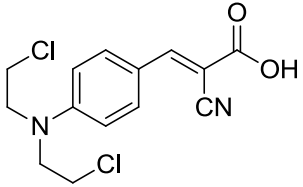
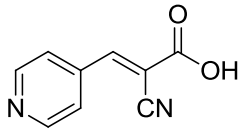
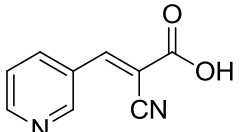
	Compound Number	Starting Material (mmol)	Product (mmol)	Yield
	<b>1</b>	10	8.5	85%

	<b>2</b>	10	9	90%
	<b>3</b>	10	8.8	88%
	<b>4</b>	10	8.5	85%
	<b>5</b>	10	8.8	88%
	<b>6</b>	10	8.6	86%
	<b>7</b>	10	8.5	85%
	<b>8</b>	10	8.7	87%
	<b>9</b>	10	8.9	89%

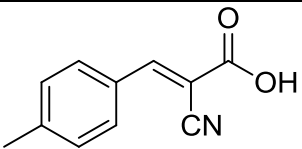
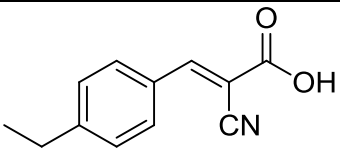
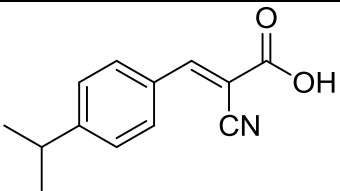
	<b>10</b>	10	8.7	87%
	<b>15</b>	10	8.5	85%

**Table 8:** Product yields from procedure 2 along with amount of starting material used and the amount of final product formed (continued on next page)

	Compound	Starting Material (mmol)	Product (mmol)	Yield
	<b>14</b>	10	9	90%
	<b>16</b>	10	8.8	88%
	<b>17</b>	10	8.7	87%

	<b>18</b>	10	8.7	87%
	<b>19</b>	10	8.5	85%
	<b>20</b>	10	8.4	84%

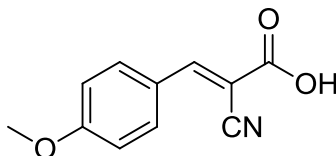
**Table 9:** Product yields from procedure 3 along with amount of starting material used and final yield

	Compound	Starting Material (mmol)	Product (mmol)	Yield
	<b>11</b>	10	9	90%
	<b>12</b>	10	9	90%
	<b>13</b>	10	8.5	85%

## **BIOLOGICAL EVALUATION:**

All the synthesized compounds were evaluated for their ability to inhibit MCT1 to transport lactate. To study this we used  $^{14}\text{C}$  lactate uptake studies. In this MCT inhibition assay rat brain endothelial 4 (RBE4) cell lines were used. RBE4 cell lines are ideal as they contain a high level of MCT1. In a 24-well plate  $2 \times 10^5$  cells/well were plated and incubated in 5%  $\text{CO}_2$  atmosphere for 16-24 hours. The cells were washed with HEPES buffer. The buffer was removed and the test compounds were added to the plate along with  $^{14}\text{C}$  lactate solution and were allowed to influx for 15 minutes. After 15 minutes the test compounds were removed and stop buffer was added to the plate. The cells were then lysed with 0.1M triton-X solution. Uptake values of the lysed cells were obtained in disintegrations per minute (dpm) using a scintillation counter. Compounds showing promising activity were studied further in low concentration and the experiment was repeated. For highly active compounds the  $\text{IC}_{50}$  values were calculated. Lactate uptake values of synthesized compounds were compared to the lactate uptake values of CHC at a concentration of  $100\mu\text{M}$ .

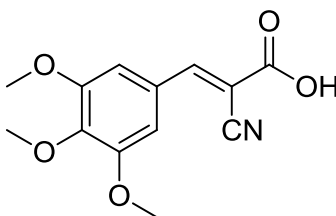
## SPECTRAL CHARACTERIZATION:



**1**

**(E)-2-cyano-3-(4-methoxyphenyl)acrylic acid 1**, Yield (85%): Yellow solid

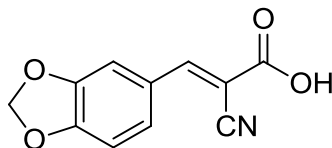
$^1\text{H}$  NMR (500MHz, DMSO d6)  $\delta$  8.16 (s, 1H), 7.98 (d,  $J=10$  Hz, 2H), 7.06 (d,  $J=10$  Hz, 2H), 3.82 (s, 3H);  $\delta$   $^{13}\text{C}$  (125MHz, DMSO d6)  $\delta$  164.46, 163.91, 154.45, 133.88, 124.68, 117.34, 115.46, 100.19, 56.28



**2**

**(E)-2-cyano-3-(3,4,5-trimethoxyphenyl)acrylic acid 2**, Yield (90%): Yellow solid: mp 211.6-213.2  $^{\circ}\text{C}$

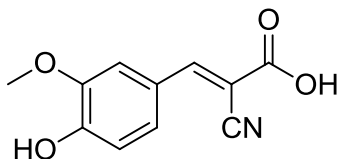
$^1\text{H}$  NMR (500MHz, DMSO d6)  $\delta$  8.25 (s, 1H), 7.46 (s, 2H), 3.79 (s, 6H), 3.68 (s, 3H);  $^{13}\text{C}$  NMR (125 MHz, DMSO d6)  $\delta$  164.151, 155.041, 153.547, 142.412, 127.197, 117.333, 117.197, 109.277, 102.624, 60.994, 56.673. Anal. Calcd. for  $\text{C}_{13}\text{H}_{13}\text{NO}_5$  (263) C, 59.31; H, 4.98; N, 5.32; found C, 59.25; H, 4.63; N, 5.33.



3

**(E)-3-(benzo[d][1,3]dioxol-5-yl)-2-cyanoacrylic acid 3:** Yield (88%): Yellow solid: mp 221.8-226.1 °C

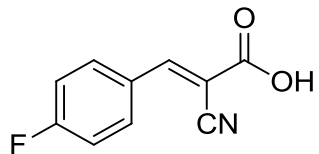
<sup>1</sup>H NMR (500MHz, DMSO d6) δ 8.19 (s, 1H), 7.71 (s, 1H), 7.51 (d, *J*=10 Hz, 1H), 7.02 (d, *J*=10 Hz, 1H), 6.15 (s, 2H); <sup>13</sup>C (125MHz, DMSO) δ 164.22, 154.23, 125.57, 148.94, 129.79, 126.26, 116.36, 108.84, 108.27, 102.84, 100.27. Anal. Calcd. for C<sub>11</sub>H<sub>7</sub>NO<sub>4</sub> (217) C, 60.83; H, 3.25; N, 6.45; found C, 60.73; H, 3.41; N, 6.47.



4

**(E)-2-cyano-3-(4-hydroxy-3-methoxyphenyl)acrylic acid 4,** Yield (85%): White solid: mp 195.8-202.8 °C

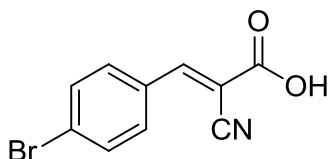
<sup>1</sup>H NMR (500MHz, DMSO d6) δ 8.06 (s, 1H), 7.63 (s, 1H), 7.49 (d, *J*=7 Hz, 1H), 6.84(d, *J*=7 Hz, 1H), 3.78 (s, 3H) <sup>13</sup>C (125 Hz, DMSO d6) δ 164.66, 154.93, 152.91, 148.39, 127.55, 123.62, 117.70, 116.58, 114.33, 98.97, 56.15. Anal. Calcd. for C<sub>11</sub>H<sub>9</sub>NO<sub>4</sub> (219) C, 60.27; H, 4.14; N, 6.39; found C, 60.14; H, 3.66; N, 6.12.



5

**(E)-2-cyano-3-(4-fluorophenyl)acrylic acid 5**, Yield (88%): White solid

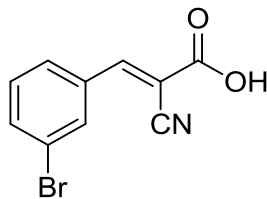
$^1\text{H}$  NMR (500MHz, Acetone d6)  $\delta$  8.30 (s, 1H), 8.09 (d,  $J=15$  Hz, 2H), 7.39 (d,  $J=15$  Hz, 2H);  $^{13}\text{C}$  NMR (125MHz, Acetone d6)  $\delta$  166.17, 163.87, 153.68, 134.07, 128.88, 117.25, 116.67, 104.5



6

**(E)-3-(4-bromophenyl)-2-cyanoacrylic acid 6** Yield (86%): White solid: mp 209.0-211.0  $^{\circ}\text{C}$

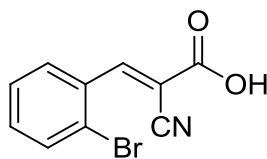
$^1\text{H}$  NMR (500MHz, DMSO d6)  $\delta$  8.31 (s, 1H), 7.94 (d,  $J=8.5$  Hz, 2H), 7.78 (d,  $J=8.5$  Hz, 2H);  $^{13}\text{C}$  NMR (125MHz, DMSO d6)  $\delta$  163.75, 153.84, 133.06, 133.01, 131.40, 127.54, 116.57, 105.21. Anal. Calcd. for  $\text{C}_{10}\text{H}_6\text{BrNO}_2$  (251) C, 47.65; H, 2.40; N, 5.56; found C, 47.60; H, 1.21; N, 6.06.



**7**

**(E)-3-(3-bromophenyl)-2-cyanoacrylic acid 7**, Yield (85%): White solid

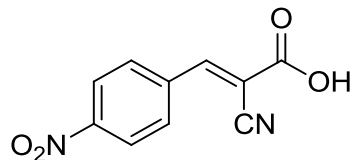
$^1\text{H}$  NMR (500MHz, DMSO  $d_6$ )  $\delta$  8.34 (s, 1H), 8.21 (s, 1H), 8.02 (d, 1H), 7.80 (d, 1H), 7.54 (t,  $J=10$  Hz, 1H);  $^{13}\text{C}$  NMR (125MHz, DMSO  $d_6$ )  $\delta$  163.56, 153.38, 136.05, 134.50, 133.60, 131.98, 129.89, 122.97, 116.41, 106.23



**8**

**(E)-3-(2-bromophenyl)-2-cyanoacrylic acid 8**, Yield (87%): White solid

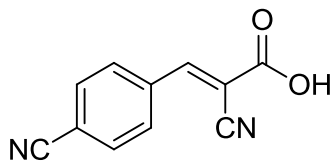
$^1\text{H}$  NMR (500MHz, Methanol  $d_4$ )  $\delta$  8.59 (s, 1H), 8.14 (d,  $J=7.1$  Hz, 1H), 7.78 (d,  $J=7.1$  Hz, 1H), 7.55-7.48 (m, 2H)  $^{13}\text{C}$  NMR (125 MHz, Methanol  $d_4$ )  $\delta$  163.05, 153.23, 133.64, 133.56, 132.12, 130.01, 128.06, 125.72, 114.70



**9**

**(E)-2-cyano-3-(4-nitrophenyl)acrylic acid 9** Yield (89%): Yellow solid

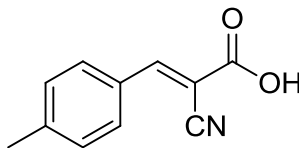
$^1\text{H}$  NMR (500MHz, Acetone d6)  $\delta$  8.45 (s, 1H), 8.405 (d,  $J=5$  Hz, 2H), 8.24 (d,  $J=10$  Hz, 2H);  $^{13}\text{C}$  NMR (125MHz, Acetone d6)  $\delta$  162.82, 151.94, 149.84, 137.82, 131.57, 124.04, 115.08, 108.09



**10**

**(E)-2-cyano-3-(4-cyanophenyl)acrylic acid 10** Yield (87%): White solid: mp 234.2-235.3  $^{\circ}\text{C}$

$^1\text{H}$  NMR (500MHz, DMSO d6)  $\delta$  8.16 (s, 1H), 7.945 (d,  $J=8.5$  Hz, 2H) 6.92 (d  $J=8$  Hz, 2H);  $^{13}\text{C}$  NMR (125Hz DMSO d6)  $\delta$  164.71, 163.23, 154.74, 134.35, 123.33, 117.61, 116.99, 99.10



**11**

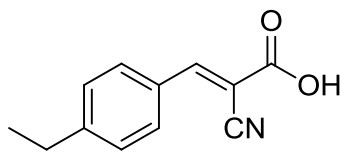
**(E)-2-cyano-3-(p-tolyl)acrylic acid 11** Yield (90%) White solid: mp 201.0-205.2 °C

<sup>1</sup>H NMR (500 MHz DMSO d6) δ 8.20 (s, 1H), 7.87 (s, 2H), 7.32 (s, 2H), 2.34 (s, 3H);

<sup>13</sup>C NMR (125 MHz DMSO d6) δ 164.13, 154.88, 144.60, 131.44, 130.53, 129.49,

116.49, 102.97, 21.96. Anal. Calcd. for C<sub>11</sub>H<sub>9</sub>NO<sub>2</sub> (187.1) C, 70.58; H, 4.85; N, 7.48;

found C, 69.78; H, 3.51; N, 7.52.



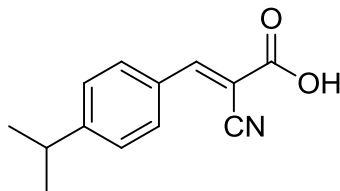
**12**

**(E)-2-cyano-3-(4-ethylphenyl)acrylic acid 12** Yield (90%) White solid: mp 159.8-162.8 °C

<sup>1</sup>H NMR (500 MHz DMSO d6) δ 8.24 (s, 1H), 7.92 (d, *J*=8.5 Hz, 2H), 7.36 (d, *J*=8.5 Hz, 2H), 2.64 (q, *J*=8, 15.5 Hz, 2H), 1.16 (t, *J*=8 Hz, 3H); <sup>13</sup>C NMR (125 MHz DMSO d6) δ

164.13, 154.92, 150.62, 131.57, 129.75, 129.36, 116.91, 103.06, 28.99, 15.66. Anal.

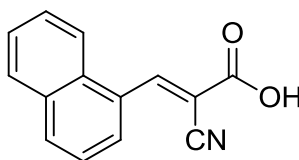
Calcd. for C<sub>12</sub>H<sub>11</sub>NO<sub>2</sub> (201) C, 71.63; H, 5.51; N, 6.96; found C, 71.53; H, 5.82; N, 7.08.



**13**

**(E)-2-cyano-3-(4-isopropylphenyl)acrylic acid 13** Yield (85%) White solid: mp 138.5-143.1 °C

<sup>1</sup>H NMR (500 MHz Methanol d<sub>4</sub>) δ 8.209 (s, 1H), 7.905 (d, *J*=7 Hz, 2H), 7.360 (d, *J*=6.5 Hz, 2H), 2.954-2.930 (m, 1H), 1.237 (s, 6H); <sup>13</sup>C NMR (125 MHz Methanol d<sub>4</sub>) δ 164.137, 154.927, 150.621, 131.573, 129.757, 129.361, 116.915, 103.067, 28.998, 15.662. Anal. Calcd. for C<sub>13</sub>H<sub>13</sub>NO<sub>2</sub> (215) C, 72.54; H, 6.09; N, 6.51; found C, 73.32; H, 7.64; N, 6.76.

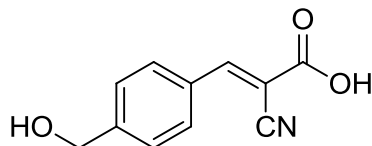


**14**

**(E)-2-cyano-3-(naphthalen-1-yl)acrylic acid 14** Yield (90%): Yellow solid: mp 198.5-202.3 °C

<sup>1</sup>H NMR (500 MHz DMSO d<sub>6</sub>) δ 9.01 (s, 1H), 8.16 (d, *J*=8.5 Hz, 1H), 8.17 (d, *J*=7 Hz, 1H), 8.05 (d, *J*=1.5 Hz, 1H), 8.03 (d, *J*=1.5 Hz, 1H), 7.65-7.61 (m, 3H); <sup>13</sup>C NMR (125 MHz DMSO d<sub>6</sub>) δ 163.65, 153.14, 133.72, 133.29, 131.45, 129.59, 129.53, 128.51,

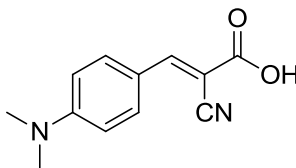
128.39, 127.62, 126.15, 124.08, 116.54, 108.84. Anal. Calcd. for C<sub>14</sub>H<sub>9</sub>NO<sub>2</sub> (223) C, 75.33; H, 4.06; N, 6.27; found C, 74.87; H, 4.48; N, 6.60.



**15**

**(E)-2-cyano-3-(4-(hydroxymethyl)phenyl)acrylic acid 15** Yield (85%): White solid:  
mp 209.0-211.0 °C

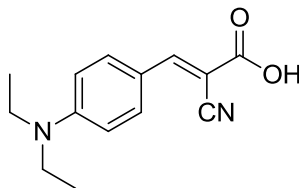
<sup>1</sup>H NMR (500MHz, Methanol d<sub>4</sub>) δ 8.28 (s, 1H), 8.004 (d, *J*=8 Hz, 2H), 7.53 (d, *J*=8 Hz, 2H), 5.06 (s, 2.29); <sup>13</sup>C NMR (125 Hz, Methanol d<sub>4</sub>) δ 164.04, 154.46, 147.69, 130.97, 130.97, 130.81, 127.12, 115.90, 63.37.



**16**

**(E)-2-cyano-3-(4-(dimethylamino)phenyl)acrylic acid 16** Yield (88%): Yellow solid:  
mp 202.0-203.3 °C

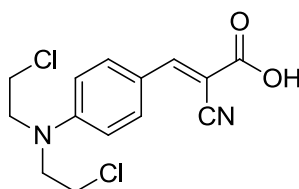
<sup>1</sup>H NMR (500 MHz, DMSO d<sub>6</sub>) δ 13.29 (s, 1H), 8.03 (s, 1H), 7.92 (d, *J*=9.5 Hz, 2H), 6.33 (d, *J*=9 Hz, 2H), 3.06 (s, 6H); <sup>13</sup>C NMR (125 MHz, DMSO d<sub>4</sub>) δ 165.56, 154.54, 154.21, 134.22, 119.11, 118.66, 112.37, 94.15. Anal. Calcd. for C<sub>12</sub>H<sub>12</sub>N<sub>2</sub>O<sub>2</sub> (216) C, 66.65; H, 5.59; N, 12.96; found C, 66.07; H, 4.86; N, 12.75.



17

**(E)-2-cyano-3-(4-(diethylamino)phenyl)acrylic acid 17** Yield (87%) Yellow solid:  
166.9-167.5 °C

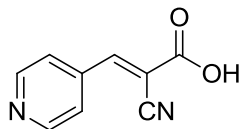
<sup>1</sup>H NMR (500 MHz DMSO d6) δ 8.02 (s, 1H), 7.9 (d, *J*=10 Hz, 2H), 6.78 (d, *J*=10 Hz, 2H), 3.44 (q, *J*=5, 16 Hz, 4H), 1.11 (t, *J*=10 Hz, 6H); <sup>13</sup>C NMR (125 MHz DMSO d6) δ 165.64, 154.29, 152.07, 134.59, 118.73, 118.61, 111.98, 93.47, 13.08. Anal. Calcd. for C<sub>14</sub>H<sub>16</sub>N<sub>2</sub>O<sub>2</sub> (224) C, 68.83; H, 6.60; N, 11.47; found C, 68.73; H, 8.18; N, 11.43.



18

**(E)-3-(4-(bis(chloromethyl)amino)phenyl)-2-cyanoacrylic acid 18** Yield (87%)  
Yellow solid: mp 197.3-198.5 °C

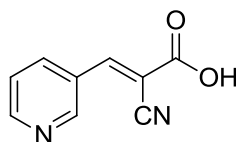
<sup>1</sup>H NMR (500 MHz Methanol d4, Acetone d6) δ 8.10 (s, 1H), 7.99 (d, *J*=9 Hz, 2H), 6.95 (d, *J*=9.5 Hz, 2H), 3.95 (t, *J*=6.5, 13.5, 4H), 3.80 (t, *J*=6.5, 13.5 Hz, 4H); <sup>13</sup>C NMR (125 MHz Methanol d4, Acetone d6) δ 164.92, 154.22, 151.32, 134.01, 120.72, 117.28, 112.20, 52.75, 40.52. Anal. Calcd. for C<sub>14</sub>H<sub>14</sub>Cl<sub>2</sub>N<sub>2</sub>O<sub>2</sub> (312) C, 53.69; H, 4.51; N, 8.94; found C, 53.22; H, 2.68; N, 8.42.



**19**

**(E)-2-cyano-3-(pyridin-4-yl)acrylic acid 19** Yield (87%) White solid: mp 180.7-180.9

$^1\text{H}$  NMR (500MHz DMSO  $d_6$ )  $\delta$  8.815 (d,  $J=4.5$  Hz, 2H), 8.372 (s, 1H), 7.867 (d,  $J=4.5$  Hz, 2H);  $^{13}\text{C}$  NMR (125 MHz DMSO  $d_6$ )  $\delta$  163.097, 152.694, 151.420, 139.336, 123.931, 115.886, 109.793, 67.061

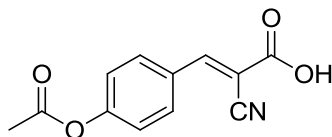


**20**

**(E)-2-cyano-3-(pyridin-3-yl)acrylic acid 20** Yield (84%): White solid: mp 204.5-205.5

$^{\circ}\text{C}$

$^1\text{H}$  NMR (500MHz, Methanol  $d_4$ )  $\delta$  9.07 (s, 1H), 8.75 (d,  $J=5$  Hz, 1H), 8.46 (d,  $J=6.5$  Hz, 1H), 8.41 (s, 1H), 7.63 (t,  $J= 5.5$  Hz, 1H);  $^{13}\text{C}$  NMR (125 MHz DMSO  $d_6$ )  $\delta$  163.43, 153.56, 152.35, 152.20, 137.14, 128.46, 124.88, 116.45, 106.99



**21**

**(E)-3-(4-acetoxyphenyl)-2-cyanoacrylic acid 21** Yield (85%) White solid: mp 186.5-189.6 °C

$^1\text{H}$  NMR (500MHz DMSO d6)  $\delta$  8.33 (s, 1H), 8.07 (d,  $J=8.5$  Hz, 2H), 7.35 (d,  $J=8.5$  Hz, 2H), 2.30 (s, 3H);  $^{13}\text{C}$  NMR (125 MHz DMSO d6)  $\delta$  169.63, 163.92, 154.44, 154.12, 132.87, 129.83, 123.58, 116.79, 104.38, 21.56. Anal. Calcd. for  $\text{C}_{12}\text{H}_9\text{NO}_4$  (231) C, 62.34; H, 3.92; N, 6.06; found C, 62.11; H, 1.92; N, 6.12.

APPENDIX:

